


Article

An Improved Droop Control Strategy Based on Changeable Reference in Low-Voltage Microgrids

Chunxia Dou ^{1,2,*}, Zhanqiang Zhang ^{1,*} , Dong Yue ² and Hanxiao Gao ³¹ Institute of Electrical Engineering, Yanshan University, Qinhuangdao 066004, China² Institute of Advanced Technology, Nanjing University of Posts and Telecommunications, Nanjing 210023, China; medongy@vip.163.com³ Institute of Marxism, Yanshan University, Qinhuangdao 066004, China; hxgaoyu@163.com

* Correspondence: cxdou@ysu.edu.cn (C.D.); zhanqiangzhangysu@163.com (Z.Z.); Tel.: +86-0335-8387556 (C.D. & Z.Z.)

Received: 10 May 2017; Accepted: 20 July 2017; Published: 26 July 2017

Abstract: This paper proposes an improved droop control strategy based on changeable reference in low-voltage microgrids. To restore running frequency of distributed generation to a rated value without affecting its reactive power output, changeable frequency reference, mainly compensating for frequency deviation, are proposed corresponding to various load demands. In terms of active power sharing inaccuracy associated with mismatched line impedance, changeable voltage amplitude reference is proposed to obtain a droop line suitable for the actual voltage of distributed generations. By further improvement of the active droop coefficient, power sharing is accurate with a difference in actual voltages of distributed generations. Virtual negative inductance is used to neutralize the redundant line inductance for strictly improving sharing accuracy. A robust control method based on Lyapunov function is used to handle the robustness problem in case of load variation. The control scheme is entirely decentralized, so communication links among distributed generations are redundant. Finally, simulation studies demonstrate the effectiveness of a control strategy.

Keywords: droop control; changeable reference; frequency deviation; active power sharing; robust control

1. Introduction

Distributed generation technology, as a research direction of new energies development, refers to distributed generation devices (DGs) resettled directly into distributed networks or near loads, including the micro-turbine, photo-voltaic cell, wind turbine and fuel cell, etc. [1,2]. For the dispersion of DGs, comprehensive management and utilization are difficult (e.g., how to minimize power supply variations properly and maintain DGs power balance) [3]. An autonomous power system consisting of various DGs, energy storage units, loads and its control system is called a microgrid and can effectively integrate DGs to maintain a stable power supply for loads [4–7]. Generally, microgrids that are small-scale low-voltage energy networks can be mainly used to ensure local generation and distribution in remote/isolated/underdeveloped communities [8]. Besides, microgrids can partially address the challenges of safe network operation and efficient power control, brought on by huge numbers of DGs, in a decentralized way and further help large grids to reduce the control burden [9].

Microgrids can work either autonomously (islanded mode) or be interconnected with large grids (grid-connected mode) [10] through power electronic devices, and for the AC microgrid, the main device is the inverter [11]. In normal operation, the microgrid is connected to the large grid, and DGs in the network can obey the large grid's dispatching to operate without being in control. In case of a disturbance, the microgrid can disconnect from the large grid and enter islanded mode, at which point DGs need to work autonomously with appropriate control methods so as to maintain power

stability. The islanded operation can bring more flexibility to the integration of DGs and provide a more reliable power supply, but islanded microgrids may become much weaker than traditional large grids for limited DGs capacities [12]. Droop control, as a common control method of interfaced inverter in islanded mode, can spontaneously coordinate the dispatched powers of DGs by controlling their respective voltages without communication among DGs [13–15]. It then implements the DGs' plug-and-play function and peer-to-peer control. However, global running frequency deviates from rated value as loads change [16]. The above frequency performance, attributed to the inherent droop feature, is hardly considered in the relevant literature. Besides, relative to bus voltage, deviation scales of DGs voltages are different for mismatched line impedance [17,18], so power-sharing inaccuracy remains to be settled [19].

A consensus-based distributed frequency control method is proposed for frequency restoration in [20]. Meanwhile the dependency on global communication links in frequency information exchange exists, so it is not absolutely decentralized. A finite-time control protocol for frequency restoration, based on feedback linearization, is proposed in order to synchronize the global frequency to nominal value with better disturbance rejection properties in [21]. The frequency deviation is corrected by droop compensation in DG self-frequency restoration control without requiring a secondary controller [22]. However, power coupling in P/f droop control, caused by resistive line impedance in low-voltage microgrids, seems not to be considered, so it is applied to high/medium-voltage microgrids. Generally, a method directly applied to low-voltage microgrids is P/U droop, but it is similarly limited to resistive line impedance (P/f droop is inductive line impedance).

In addition to frequency restoration, active power sharing inaccuracy caused by mismatched line impedance also remains to be settled. Although the two problems are settled together in some studies, they are mutually independent in P/U droop control [23]. Enhanced virtual impedance is proposed to compensate mismatched line impedance for minimizing the power sharing error [24,25]. Virtual impedance is regarded as an effective tool for improving power sharing accuracy. Power information as a small disturbance signal is injected into the system to improve power sharing accuracy based on the power error before and after injecting the signal in [26], but the stability declines. Paper [27] uses low-bandwidth synchronization signals to activate the abovementioned sharing error reduction operation. It will lead to a decrease in DG voltages so as to reduce the impacts of line impedance. However, the application of simple communication may reduce stability.

Changeable reference, used in P/U droop control, is firstly proposed in this paper to realize frequency restoration and accurate active power sharing in low-voltage microgrids. The strategy is entirely decentralized without communication links between DGs. The innovative works of this paper are as follows.

- Changeable frequency reference (CFR), suitable for frequency droop control, is proposed to restore the DG running frequency. For compensating the frequency deviation (e.g., frequency drop), the calculation of CFR is designed in an iterative way by adding real-time frequency deviation to the rated frequency. Thus, running frequency will stabilize at a rated value.
- To obtain accurate active power sharing, changeable voltage amplitude reference (CVAR) in voltage droop control is proposed. The calculation of CVAR is also designed in an iterative way by adding the real-time line voltage drop to rated voltage, so that theoretical droop lines can be converted to actual droop lines corresponding to actual voltage.
- Based on CVAR, the active droop coefficient is further improved so as to obtain a new droop line corresponding to actual DG operation. Even in the case of different DG voltages, active power sharing remains accurate. The same objective as with CVAR is realized, and voltage amplitude reference in the new droop line remains constant.
- This paper considers the inverter impedance and designs its equivalent value as a negative line inductance. The elimination of line inductance contributes to strictly accurate active power sharing. Virtual impedance is used to realize the inverter impedance design.

- Besides control precision, robustness problem is handled in inter-loop controllers by proposing a robust control method, based on the Lyapunov function that corresponds to DGs.

This paper is organized as follows. Section 2 describes the principle of P/U droop control considering inverter impedance in low-voltage microgrids. Section 3 describes the CFR-based improved frequency droop control. Section 4 describes the CVAR-based voltage droop control and further improves the active droop coefficient. Section 5 describes the related controller designs and robust control details. Section 6 gives the simulation results. Section 7 summarizes the paper and gives conclusions.

2. P/U Droop Control

For a DG in the microgrid, the equivalent circuit of its grid-connected state is shown in Figure 1, where $U_{DG} \angle \delta$ is DG voltage; S is DG powers output; $U_S \angle 0^\circ$ is bus voltage; X_L, R_L are line impedance; i_o is line current; X_I, R_I are inverter impedance whose values rely on the control demands when necessary (e.g., neutralize line inductance in this paper). The inverter impedance is not certainly a physical impedance but the equivalent impedance when the current flowing through inverter is equivalent to line current i_o . Based on the circuit in Figure 1, the power outputs of DG are

$$P = \frac{U_S}{(R_I + R_L)^2 + (X_I + X_L)^2} [(R_I + R_L)(U_{DG} \cos \delta - U_S) + (X_I + X_L)U_{DG} \sin \delta] \quad (1)$$

$$Q = \frac{U_S}{(R_I + R_L)^2 + (X_I + X_L)^2} [(X_I + X_L)(U_{DG} \cos \delta - U_S) - (R_I + R_L)U_{DG} \sin \delta] \quad (2)$$

Then, combine (1) with (2) and obtain the following equations

$$U_{DG} \sin \delta = [(X_I + X_L)P - (R_I + R_L)Q]/U_S \quad (3)$$

$$U_{DG} \cos \delta - U_S = [(R_I + R_L)P + (X_I + X_L)Q]/U_S \quad (4)$$

Impedance between DG and bus in low-voltage microgrids is mainly line resistance ($R_L \gg X_L$) [28] without considering inverter impedance, where P/U droop control is applicable. Although line inductance is insignificant, the voltage drop in line inductance associated with the values of DG voltages affects power sharing. This paper considers the inverter impedance and designs its value for fully eliminating line inductance. Thus, power sharing is strictly improved and power coupling caused by line inductance is incidentally restrained [29]. The virtual impedance method is used to design inverter impedance as given virtual impedance. For the above objective, design inverter impedance is negative line inductance: $X_I = -X_L, R_I = 0$. Hence, in the subsequent part, line inductance is unnecessary to be considered and “line impedance” is line resistance. Due to the small power angle δ , $\sin \delta = \delta, \cos \delta = 1$ are reasonably assumed. Based on (3) and (4), we can derive as

$$\delta = -(R_L Q)/(U_{DG} U_S) \quad (5)$$

$$U_{DG} - U_S = (R_L P)/U_S \quad (6)$$

Generally, power angle can be replaced by DG frequency f . Hence, P/U droop control equations of DG are obtained as

$$f = f^* - m(Q - Q^*) \quad (7)$$

$$U = U^* + n(P - P^*) \quad (8)$$

where m, n are respectively reactive and active droop coefficients, given as

$$m = (f_{\max} - f^*)/(Q^* - Q_{\max}) \quad (9)$$

$$n = (U^* - U_{\min}) / (P^* - P_{\max}) \quad (10)$$

where f^* is frequency reference whose rated value is popularly 50 Hz; U^* is voltage amplitude reference whose rated value is equal to bus voltage; Q^*, P^* are rated powers output; f_{\max} is maximum running frequency; U_{\min} is minimum voltage amplitude; Q_{\max}, P_{\max} are maximal powers capacity. As seen in (7) and (8), DG running frequency is greatly affected by load power demands. The running frequency cannot stabilize at rated values when loads change. Hence, traditional P/U droop control is poorly adjusted in the stabilization performance of running frequency, and frequency restoration is necessary. In a microgrid with mismatched line impedance, DG (e.g., DG1, DG2) voltages are unequal ($U_1 \neq U_2$) substituted into (8) and (10), and derive as $P_1/P_2 \neq n_2/n_1 = P_{\max1}/P_{\max2}$. Hence, active power sharing accuracy in traditional P/U droop control remains to be improved.

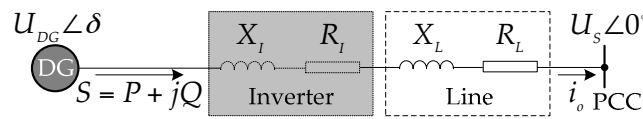


Figure 1. Equivalent circuit of grid-connected DG.

3. CFR-Based Improved Frequency Droop Control

Traditional frequency droop feature of DG is presented as line L_0 in Figure 2, where $f(t)$ is the DG running frequency, $Q(t)$ is the DG reactive power output, $\Delta f(t)$ is the running frequency deviation. Assume that DG operates at rated point O at initial state. When loads change at $t = j$, DG reactive power output changes to $Q(j)$ and the frequency deviation of running point N' relative to point O is $\Delta f(j)$. Obviously, when loads change, the running frequency cannot stabilize at a rated value. So the frequency regulation in traditional droop control is a deviating regulation. To restore the running frequency to a rated value, CFR is proposed to compensate the frequency deviation (i.e., frequency reference increases/reduces as much as running frequency reduces/increases). The CFR value determination is related to the variation value of the DG reactive power output. That is, the value of CFR changes with loads. For any DG, detailed determination steps of CFR are as follows:

1. Determine the variation values of DG reactive power output.

Assume loads change at moments $t = 1, 2, \dots, j, \dots, n$ ($j \geq 2$). Relative to reactive power output of DG at $t = j - 1$, the variation value of DG reactive power output at $t = j$ is

$$\Delta Q(j) = Q(j) - Q(j-1) \quad (11)$$

When loads increase, $\Delta Q(j) > 0$, otherwise, $\Delta Q(j) < 0$. Define $\Delta Q(0) = 0$ (corresponding to DG assumed to run on non-load state at $t = 0$ s, otherwise, it can be defined widely), the variation vector of DG reactive power output at $(n+1)$ moments, set to \mathbf{Q} , is given as

$$\mathbf{Q} = (\Delta Q(0), \Delta Q(1), \dots, \Delta Q(j), \dots, \Delta Q(n))^T \quad (12)$$

2. Determine the compensation values of frequency reference.

Based on (7) and (11), the running frequency deviation at $t = j$ is

$$\Delta f(j) = -m \cdot \Delta Q(j) \quad (13)$$

Since $m < 0$, $\Delta f(j) > 0$ when $\Delta Q(j) > 0$, otherwise, $\Delta f(j) < 0$ when $\Delta Q(j) < 0$. The running frequency is proportional to DG reactive power output. Set the frequency reference at $t = j$ as:

$$\Delta f^*(j) = f^*(j) - f^*(j-1) = -\Delta f(j) \quad (14)$$

According to (11)–(14), it is clear that when loads reduce/increase at $t = j$, the frequency reference increases/reduces as much as the running frequency deviation reduces/increases. The compensation vector of frequency references, set to R , is given as

$$R = mQ \quad (15)$$

3. Determine the frequency references at $(n + 1)$ moments.

Set the vector of frequency references to F :

$$F = (f^*(0), f^*(1), \dots, f^*(j), \dots, f^*(n))^T \quad (16)$$

where $f^*(0) = 50 - mQ^*$ is also defined. Based on (14), we can obtain (17)

$$F = MF + R \quad (17)$$

where M is a constant matrix with $(n + 1)$ -dimensions and the rank is n ($\text{rank}(M) = n$), given as

$$M = \begin{bmatrix} 1 & 0 & \cdots & 0 & 0 \\ 1 & 0 & \cdots & 0 & 0 \\ 0 & 1 & \cdots & 0 & 0 \\ \vdots & \vdots & \ddots & \vdots & \vdots \\ 0 & 0 & \cdots & 1 & 0 \end{bmatrix}_{(n+1) \times (n+1)} \quad (18)$$

Frequency references at $(n + 1)$ moments as elements constitute the solution space F of following nonhomogeneous linear equation:

$$(E - M)F = mQ \quad (19)$$

where E is an identity matrix with $(n + 1)$ -dimensions. Although the rank of coefficient matrix $E - M$ is n ($\text{rank}(E - M) < n + 1$), the solution space of (19) is still definite for an initial condition $f^*(0) = 50 - mQ^*$ (i.e., special solution). The CFR calculation is similar to an iteration process of (14) with the initial value: $50 - mQ^*$. Due to the uncertainty of load changes, it is preferential to obtain the frequency reference at the current running moment. Even in case of continuous or frequent load variations, the proposed CFR calculation at all load change moments is feasible, otherwise, use (14) directly to calculate the frequency reference at the current running moment.

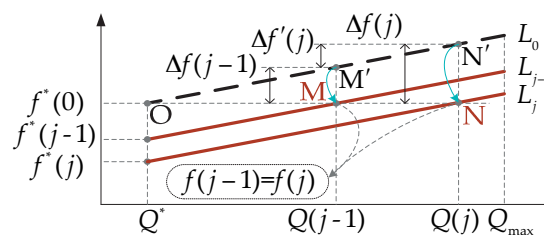


Figure 2. CFR-based frequency droop features of DG.

As shown in Figure 2, lines L_{j-1}, L_j are the CFR-based improved frequency droop lines at $t = j - 1, j$. In addition, the corresponding running points are M, N changed from points M', N' . Relative to point O , frequency references reduce as much as original frequency increases ($\Delta f(j - 1), \Delta f(j)$). When loads change at $t = j$, DG reactive power output is changed from $Q(j - 1)$ to $Q(j)$ and frequency reference is changed from $f^*(j - 1)$ to $f^*(j)$ according to (14). If frequency reference remains constant at $t = j$, the frequency deviation $\Delta f'(j)$ will exist. Line L_j is necessary to serve as frequency droop line at $t = j$. So frequency references should be changeable with load variations to stabilize running frequency. Thus, running frequency hardly changes when loads change

at $t = j$ ($f(j-1) = f(j)$). Hence, within the allowable range of DG reactive power output, running frequency can be maintained at 50 Hz no matter how loads change.

4. CVAR-Based Improved Voltage Droop Control

4.1. CVAR Determination

Active power sharing in accordance with DG power capacity largely depends on whether DG voltages are consistent. However, there are unequal line voltage drops between actual DG voltages and bus voltage associated with mismatched line impedance, so that values of actual voltages are slightly larger than theoretical values. Theoretical voltage droop lines so not satisfy actual voltages. If we still use the theoretical voltage droop lines to control DGs, active power sharing will be inaccurate for different actual voltages caused by unequal line voltage drops. Hence, line voltage drops are considered to improve voltage droop features by proposing CVAR when loads change. The principle of CVAR is adding line voltage drop to rated voltage amplitude reference, so that theoretical droop lines can be converted to actual droop lines corresponding to actual voltages. Only when droop lines are suitable for actual voltages will active power sharing be accurate in the case of discrepant DG voltages. This paper considers the inverter impedance and designs it as negative line inductance, so following “line voltage drop” refers to voltage drop in line resistance. For any DG in a microgrid, the detailed determination steps of CVAR are as follows:

1. Determine the variation values of “line voltage drop”.

Assume loads also change at moments $t = 1, 2, \dots, j, \dots, n$ ($j \geq 2$). Relative to the “line voltage drop” at $t = j - 1$, the variation value of “line voltage drop” at $t = j$ is

$$\Delta U_L(j) = U_L(j) - U_L(j-1) \quad (20)$$

For line current increases as loads increase, $\Delta U_L(j) > 0$, otherwise, $\Delta U_L(j) < 0$. Define $\Delta U_L(0) = 0$ (corresponding to DG assumed to run on non-load state at $t = 0$ s, otherwise, it can be defined widely), the variation vector of “line voltage drop” at $(n+1)$ moments, set to O , is given as

$$O = (\Delta U_L(0), \Delta U_L(1), \dots, \Delta U_L(j), \dots, \Delta U_L(n))^T \quad (21)$$

2. Determine the voltage amplitude references at $(n+1)$ moments.

Set the DG voltage amplitude reference at $t = j$ to

$$U^*(j) = U^*(j-1) + \Delta U_L(j) \quad (22)$$

According to (20) and (22), it is clear that when loads reduce/increase at $t = j$, voltage amplitude reference reduces/increases as much as “line voltage drop” reduces/increases. The vector of voltage amplitude references at $(n+1)$ moments, set to U , is given as

$$U = (U^*(0), U^*(1), \dots, U^*(j), \dots, U^*(n))^T \quad (23)$$

where $U^*(0)$ (i.e., voltage amplitude reference at initial time or no-load running state) is generally the bus voltage ($U^*(0) = U_S$). Based on (22), there is

$$U = MU + O \quad (24)$$

where M is shown in (18). Voltage amplitude references at $(n+1)$ moments as elements constitute the solution space U of following nonhomogeneous linear equation:

$$(E - M)U = O \quad (25)$$

The coefficient matrix in (25) is the same with (19), so the solution space of (25) is also definite for an initial condition $U^*(0) = U_s$, i.e., special solution.

Voltage droop features are shown in Figure 3, where line l_0 is the traditional/theoretical droop line at $t = 0$; lines l_1, l_2 are the CVAR-based improved droop lines at $t = j - 1, j$; line l_3 is also the improved droop line corresponding to maximum active power running point P; $U'(t)$ is the DG actual voltage; $P(t)$ is the DG active power output; $U_L(t)$ is the ‘line voltage drop’. Because the ‘line voltage drop’ exists at $t = j - 1, j$, running points are changed from points A', B' to points A, B dissatisfied with line l_0 . If we still use line l_0 to control actual voltage, active power output will deviate from theoretical value. Considering impact of ‘line voltage drop’, design voltage amplitude references at $t = j - 1, j$, so that actual droop lines l_1, l_2 conforming to actual voltages are obtained. If we use lines l_1, l_2 to control actual voltages, active power outputs will return to the exact value.

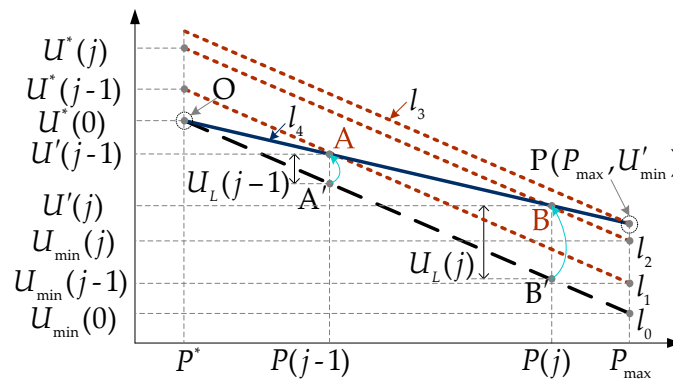


Figure 3. CVAR-based voltage droop features of DG.

4.2. CVAR-Based Active Droop Coefficient Improvement

When loads change at $t = j$, the actual running point will change from A to B and the corresponding droop line will also become line l_2 . So line l_1 is only applied to actual running point A at $t = j - 1$ and cannot cover all the DG running points at $(n + 1)$ moments (e.g., point B). When loads change, all the actual DG running points do not synchronously meet the identical improved droop line with the same voltage amplitude reference. There are $(n + 1)$ droop lines that respectively correspond to $(n + 1)$ running states at $(n + 1)$ moments. Namely, DG at different running states has different droop lines. To further improve CVAR-based droop control, a line applicable to all the actual DG running points is derived as line l_4 in Figure 3, which is proved in subsequent part. The equation is deduced as follows:

1. Determine the coordinate of point P (P_{\max}, U'_{\min}) when DG dispatches maximum active power.

The ‘line impedance’ in proposed low-voltage microgrid using virtual negative inductance is line resistance. Based on (6), when DG dispatches maximum active power, ‘line voltage drop’ is

$$U_{L-P_{\max}} = P_{\max}(R_L/U^*) \quad (26)$$

Hence, the y-axis of point P is

$$U'_{\min} = U_{\min} + U_{L-P_{\max}} \quad (27)$$

Thus, the coordinate of point P is ($P_{\max}, U_{\min} + U_{L-P_{\max}}$).

2. Determine the equation of line l_4 .

The coordinate of DG no-load running point O is (P^*, U^*). Based on coordinates of two points in line l_4 and (10), the line equation is deduced as

$$U' = U^* - nP^* + n'P \quad (28)$$

where U' is DG actual voltage, n' is the improved active droop coefficient :

$$n' = n + R_L/U^* \quad (29)$$

Based on (6), the 'line voltage drop' at a random moment (e.g., $t = j$) is

$$U_L(j) = P(j)(R_L/U^*) \quad (30)$$

Based on (8), DG actual voltage at $t = j$ is

$$\begin{aligned} U'(j) &= U(j) + U_L(j) = U^* + n(P(j) - P^*) + P(j)(R_L/U^*) \\ &= U^* - nP^* + [n + (R_L/U^*)]P(j) = U^* - nP^* + n'P \end{aligned} \quad (31)$$

From (28) to (31), it is deduced that the coordinates of actual DG running points as loads change synchronously satisfy the equation of line l_4 , so it is summarized as the actual voltage droop line. It is worth noting that voltage amplitude reference in actual voltage droop line just remains at the rated value (i.e., bus voltage).

4.3. Improved Active Power Sharing

For a microgrid with multiple parallel DGs (e.g., DG1, DG2), difference in DGs actual voltages based on (28) is

$$U'_1 - U'_2 = [n_1 + (R_{L1}/U^*)]P_1 - [n_2 + (R_{L2}/U^*)]P_2 - n_1P_1^* + n_2P_2^* \quad (32)$$

According to (6), DGs actual voltages can be expressed as

$$U'_i = U^* + (R_{Li}/U^*)P_i \quad (i = 1, 2) \quad (33)$$

We can substitute (10) and (33) into (32) and deduce as

$$(P_1 - P_1^*)/(P_2 - P_2^*) = n_2/n_1 \quad (34)$$

Hence, in case of discrepant DGs actual voltages, accurate active power sharing of DGs controlled by line l_4 is proved.

Performance of improved active power sharing in accordance with DG active power capacity is shown in Figure 4, where l'_0, l''_0 are the traditional droop lines of DG1, DG2. When lines l'_0, l''_0 are used for active power sharing and "line voltage drop" isn't considered, the active power sharing ($P_1 : P_2$) is accurate for equal voltages. However, the significant "line voltage drop" has to be considered, so DG actual voltages are discrepant (U'_1, U'_2). If we still use lines l'_0, l''_0 to control DGs, actual active power sharing ($P'_1 : P'_2$) will deviate from accurate value ($P_1 : P_2$). Lines l'_4, l''_4 are the CVAR-based improved droop lines of DG1, DG2. If they are used for active power sharing, the improvement of active droop coefficient restores DG active power output back to accurate value without changing actual DG voltages. So it is unnecessary to consider whether DG actual voltages are consistent, and meanwhile, performance of active power sharing is relatively fine.

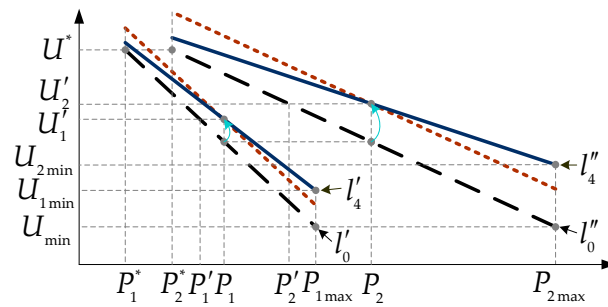


Figure 4. Improved active power sharing of DGs.

5. Control System of Improved Droop-Controlled Inverter

The control system of an improved droop-controlled inverter in a low-voltage microgrid, realized for frequency restoration and accurate active power sharing, is shown in Figure 5, where L_f is filter inductance, C_f is filter capacitor. Input capacitor voltage v_o and line current i_o assess the power calculation mode and obtain DG active/reactive power outputs. Then, the droop controller realizes the CFR/CVAR-based improved P/U droop control and sends “order voltage” v_r to a virtual controller. Generally, in a virtual controller, one must subtract the virtual voltage drop from the “order voltage” to realize virtual impedance [30,31] and then obtain a new “order voltage” v . In the inter-loop controller, robust control is used to realize that capacitor voltage tracks a new “order voltage” with minimum robustness problem in case of load variations. Pulse width modulation (PWM) mode modulates the waveform of the inverter voltage.

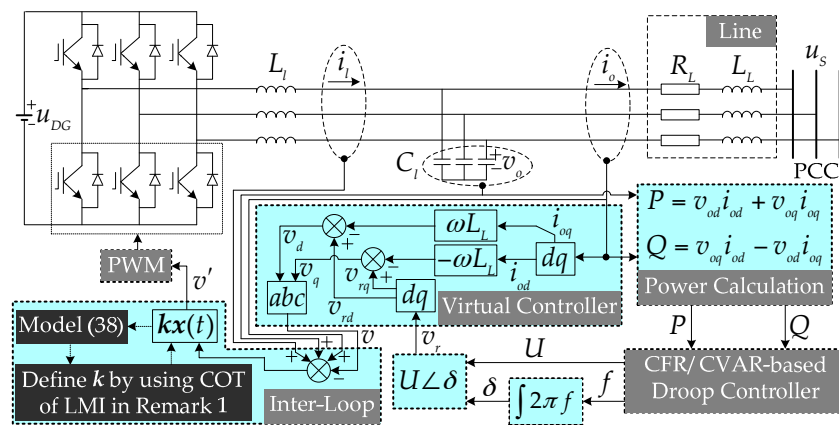


Figure 5. Improved control system of DG in low-voltage microgrid.

5.1. CFR/CVAR-Based Droop Controller Design

Figure 6 describes the detailed design of a droop controller. Based on (19) and (25), the calculation systems of CFR and CVAR are established, and CVAR calculation is replaced by a control pattern designed as (28). The iteration calculation of references relies on the established database, which is used to extract and store related physical information such as DG active/reactive power, and frequency references. The DG active/reactive powers outputted from power calculation mode are immediately stored in the database after per loads change. Then, the database extracts previously stored information (DG powers output before loads change) and obtains variation values of DG powers. The previous references necessary for reference calculation also need to be extracted. Then, new references can be obtained to contribute to an improved droop control, and meanwhile, they will be stored to the database in time for preparing the next reference calculation in advance. The application of the control

Lyapunov function is proposed corresponding to actual DGs. The following section will describe the stabilization design method.

Based on the structure diagram of the DG unit given in Figure 7, the mathematical model of the DG unit applying Kirchhoff laws is formulated as follows

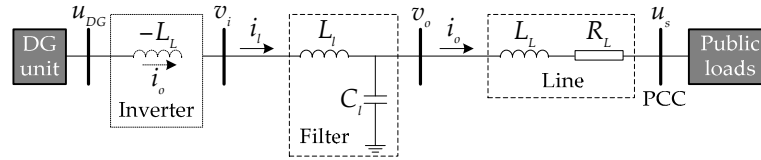


Figure 7. Structure of DG unit.

$$\begin{cases} \frac{d\Delta i_l}{dt} = -\frac{1}{L_l}\Delta v_o + \frac{1}{L_l}\Delta v_i \\ \frac{d\Delta i_o}{dt} = -\frac{R_L}{L_L}\Delta i_o + \frac{1}{L_L}\Delta v_o - \frac{1}{L_L}\Delta u_S \\ \frac{d\Delta v_o}{dt} = \frac{1}{C_l}\Delta i_l - \frac{1}{C_l}\Delta i_o \end{cases} \quad (37)$$

Considering uncertainties of loads change and line/filter parameters, the dynamic model of the DG unit as (37) might be expanded into the following form

$$\begin{cases} \dot{x}(t) = Ax(t) + Bu(t) + D\omega(t) \\ z(t) = Cx(t) \end{cases} \quad (38)$$

where $x(t) = [\Delta i_l \quad \Delta i_o \quad \Delta v_o]^T$ is state matrix of the DG unit; $u(t) = \Delta v_i$ is control input; $z(t) = \Delta v_o$ is control output; $\omega(t) = \Delta u_S$ is assumed to be a disturbance signal preferably set to zero; A , B , C and D are coefficient matrices with appropriate dimensions.

$$A = \begin{bmatrix} 0 & 0 & -\frac{1}{L_l} \\ 0 & -\frac{R_L}{L_L} & \frac{1}{L_L} \\ \frac{1}{C_l} & -\frac{1}{C_l} & 0 \end{bmatrix}, \quad B = \begin{bmatrix} \frac{1}{L_l} \\ 0 \\ 0 \end{bmatrix}, \quad C = [0 \quad 0 \quad 1], \quad D = \begin{bmatrix} 0 \\ -\frac{1}{L_L} \\ 0 \end{bmatrix}. \quad (39)$$

Then, the inter-loop controller of the DG unit in Figure 5 is designed as state feedback control

$$u(t) = kx(t) \quad (40)$$

where k is the control gain of the inter-loop controller.

Based on (38) and (40), the dynamical model of the DG unit is rearranged in the following form

$$\begin{cases} \dot{x}(t) = \bar{A}x(t) + D\omega(t) \\ z(t) = Cx(t) \end{cases} \quad (41)$$

where $\bar{A} = A + Bk$.

We define the Lyapunov function for the control system as

$$V(t) = x^T(t)Px(t) \quad (42)$$

where P is the symmetric positive definite weighting matrix of DG.

Considering the initial condition, H_∞ performance related to the controlled output is given as

$$\int_0^{t_f} z^T(t)z(t)dt \leq \rho^2 \int_0^{t_f} \omega^T(t)\omega(t)dt + V(0) \quad (43)$$

where ρ is a prescribed attenuation level. Physical meaning of (43) is minimizing impact of $\omega(t)$ on output $z(t)$, scilicet, impact of disturbance (loads variation) on tracking error in the inter-loop controller is attenuated below a desired level.

Theorem 1. *The controlled unit (41) can be H_∞ robust stabilization by the inter-loop controller (40), only if $P = P^T > 0$ is the common solution of the following symmetric matrix inequality.*

$$\begin{bmatrix} P\bar{A} + \bar{A}^T P & PD \\ D^T P & -\rho^2 I \end{bmatrix} \leq 0 \quad (44)$$

where I is an identity matrix.

Proof. The derivative of $V(t)$ along the trajectory of system (42) satisfies

$$\dot{V}(t) = 2x^T(t)P\bar{A} + 2x^T(t)PD\omega(t) \quad (45)$$

It is easy to obtain as

$$\int_0^{t_f} z^T(t)z(t)dt = V(0) - V(t_f) + \int_0^{t_f} [z^T(t)z(t) + \dot{V}(t)]dt \leq V(0) + \int_0^{t_f} \left\{ \begin{bmatrix} x^T(t) & \omega^T(t) \end{bmatrix} \begin{bmatrix} P\bar{A} + \bar{A}^T P & PD \\ D^T P & -\rho^2 I \end{bmatrix} \begin{bmatrix} x^T(t) & \omega^T(t) \end{bmatrix}^T + \rho^2 \omega^T(t)\omega(t) \right\} dt \quad (46)$$

□

Based on the above result, if matrix inequality (44) is satisfied, the system of (41) is H_∞ robust stabilization by inter-loop controller (40). The inequality (44) is linear matrix inequality (LMI).

Remark 1. *To obtain better robust performance, H_∞ robust stabilization control can be treated as the following minimization problem as (47), so that the H_∞ performance in (43) can be reduced as small as possible*

$$\begin{aligned} & \min \rho, \\ & \text{Subject to inequality (44).} \end{aligned} \quad (47)$$

The minimization problem in (47) can be transformed into a LMI convex optimization problem. By using convex optimization techniques (COT) of LMI, inter-loop controller control gain as well as minimization H_∞ robust performance of proposed droop control system can be obtained.

6. Simulation Results

The simulation model shown in Figure 8 has been established in a platform RT-LAB (Opal-RT Technologies Inc, Montreal, QC, Canada). The model is summarized as an islanded microgrid with two parallel DGs and several public loads. Simulation parameters are shown in Table 1. The improved active droop coefficients are selected by (29). Microgrid operates at no-load state at $t = 0$ s. DGs share the powers in a ratio of 1:1. To analyze the performance of reactive power/frequency and active power/DG voltage in case of load variation, simulation results are divided into three phases: increase loads (3000 W, 1000 Var) at $t = 0$ s; increase 100% of loads at $t = 1.0$ s; reduce 50% of loads at $t = 2.0$ s.

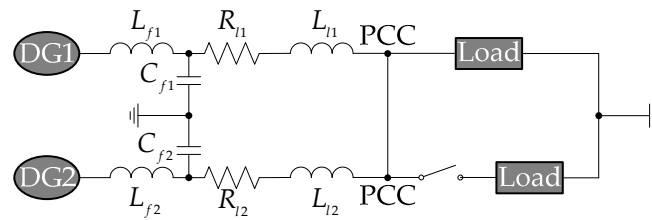


Figure 8. Single-phase equivalent circuit diagram of tested low-voltage microgrid model.

Table 1. Parameters of tested low-voltage microgrid model.

Parameter	Value (DG1)	Value (DG2)
DC voltage	700 V	700 V
Filter inductance	6 mH	6 mH
Filter capacitance	10 μ F	10 μ F
Rated voltage amplitude	311 V	311 V
Rated frequency	50 Hz	50 Hz
Powers references	500 Var, 1500 W	500 Var, 1500 W
Reactive droop coefficient	-1×10^{-4}	-1×10^{-4}
Active droop coefficient	-5×10^{-3}	-5×10^{-3}
Improved active droop coefficient	-1.9×10^{-3}	-3×10^{-3}
Line length	1.5 km	1.0 km

6.1. Results of Reactive Power/Frequency

Figure 9 shows the performance of reactive power and frequency in case of load variation. Two methods are verified: method 1 (traditional method) uses the constant frequency reference; method 2 (proposed method) uses CFR. As seen in (1b), DG1 and DG2 dispatch rated reactive power (500 Var) during $t = 0$ s to $t = 1.0$ s when putting given loads into use. Corresponding to (1a), running frequencies of DG1 and DG2 maintain at 50 Hz during $t = 0$ s to $t = 1.0$ s. However, once total loads change after $t = 1.0$ s, running frequency stabilizing at rated value can be then lost. In detail, because frequency is proportional to DG reactive power output in (7), the frequency in method 1 (traditional method) can increase as loads increase at $t = 1.0$ s and reduce as loads reduce at $t = 2.0$ s. Corresponding to (1b), DGs reactive power sharing is, however, accurate (1:1) due to the frequency synchronization in (1a). However, one remarkable thing is that the overshoot time, about 0.7 s, is relatively long.

Similarly, in (2a), running frequency in method 2 (proposed method) has been stabilized at rated value after $t = 1.0$ s. It attributes to the contribution of CFR, whose compensation can restore running frequency to rated value (50 Hz). A sudden change of frequency reference can result in the drop/rise in running frequency at $t = 1.0$ s/2.0 s in (2a). Specifically, based on (14) or (19), frequency references of DG1 and DG2 change from 50 Hz to 49.95 Hz at $t = 1.0$ s and change from 49.95 Hz to 50.025 Hz at $t = 2.0$ s. Relative to (1a), although the values of running frequency change, frequency synchronization still remains constant. Meanwhile, the same applies to DG reactive power sharing accuracy (1:1). The overshoot time as about 0.25 s becomes significantly shorter. Due to certain different system parameters of DG1 and DG2, including unbalanced line impedance, their quick responses to load changes may also be different. Thus, in (1a) and (2a), it may result in different frequencies of DG1 and DG2 in the overshoot stage. The above analysis indicates that CFR can be used to restore running frequency without influencing DG reactive power output. In addition, robust control, used in the proposed method, can minimize the robustness problem of DG frequency and reactive power in the case of load changes or disturbances.

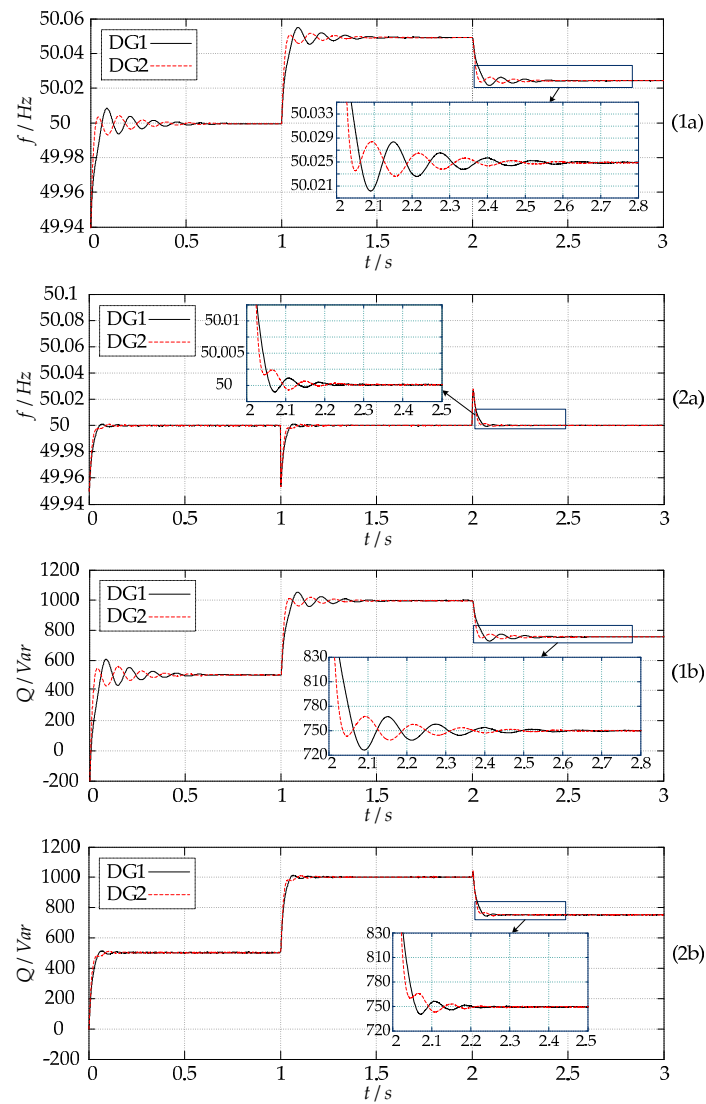


Figure 9. Simulation results of reactive power/frequency: method 1 (traditional method) using constant frequency reference; method 2 (proposed method) using CFR. (1a) DG running frequency in method 1; (2a) DG running frequency in method 2; (1b) DG reactive power output in method 1; (2b) DG reactive power output in method 2.

6.2. Results of Active Power/DG Voltage

Figure 10 shows the DG voltage deviations and active power sharing accuracy. Three methods are verified: method 1 (traditional method) uses constant voltage amplitude reference; method 2 (proposed method) uses CVAR; method 3 (proposed method) uses an improved active droop coefficient. As shown in Figure 10, because DG voltages are inversely proportional to DG active power outputs in (8), DG voltages will reduce/increase/reduce as loads increase/reduce/increase at $t = 0$ s/ $t = 1.0$ s/ $t = 2.0$ s. In method 1 (traditional method), as total loads change after $t = 0$ s, deviation in DG voltages in (1a) caused by mismatched line impedances results in active power sharing inaccuracy in (1b). In detail, when loads increase/reduce, the voltage drop in line impedance can further increase/reduce, which can result in increased/reduced DG voltage deviation in (1a) and further increase/reduce active power sharing inaccuracy in (1b). Besides, the overshoot time as about 0.6 s is also relatively long in method 1 (traditional method).

In method 2 (proposed method) using CVAR and method 3 (proposed method) using improved active droop coefficient, because voltage drop in line impedance is added into traditional voltage

amplitude reference, the DG voltages can increase in (2a) and (3a) relative to (1a). Although DG voltage deviation still exists in (2a) and (3a), the active power sharing in (2b) and (3b) are accurate by using actual voltage droop line to control DGs. Small differences in (2a) and (3a) are the obvious voltage droops/rises in (2a) for sudden reference changes. In addition, voltages in (3a) are relatively stable. The voltage droops/rises in (2a) hardly have an impact on active power sharing for the almost none droop/rise time, so sharing performances in (2b) and (3b) are almost consistent. The same applies to frequency; the overshoot time is almost nonexistent in the proposed method, attributed to robustness minimized by the proposed robustness control. Therefore, either method 2 or method 3 improves the active power sharing accuracy in case of loads variation. The above analysis indicates that CVAR or an improved active droop coefficient can be used to improve active power sharing accuracy. Besides, robust control can also minimize robustness problem of DG voltages and active power in case of load changes or disturbances.

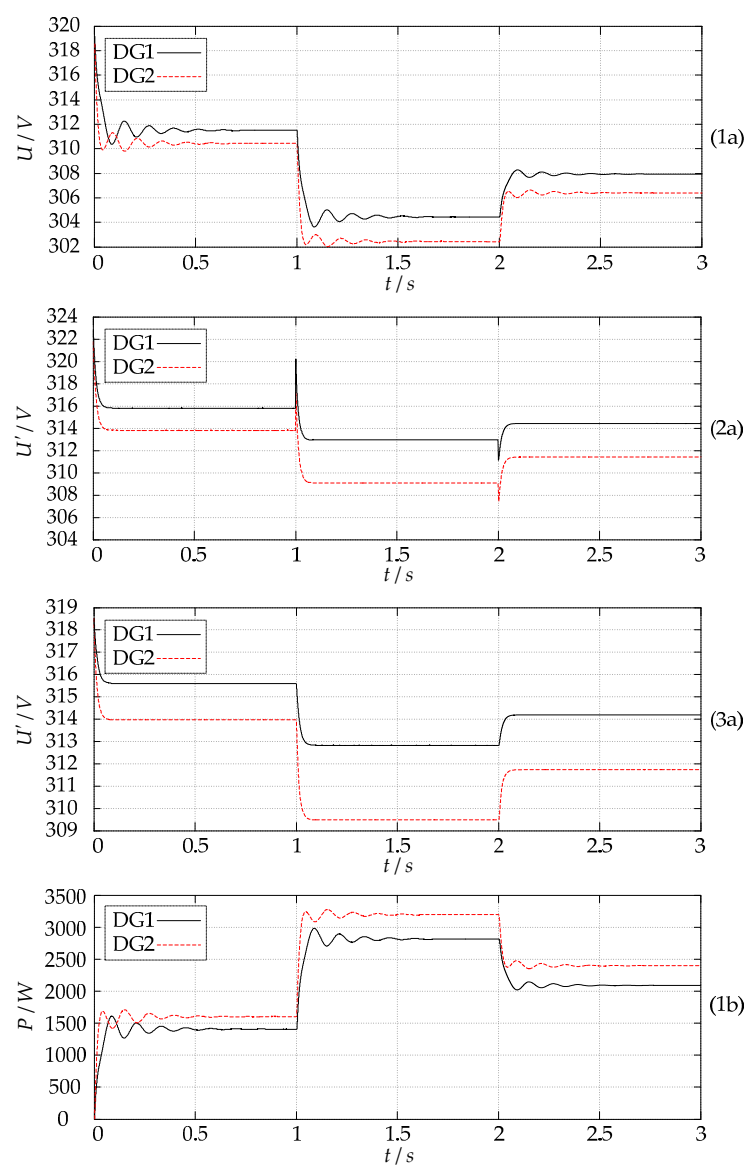


Figure 10. Cont.

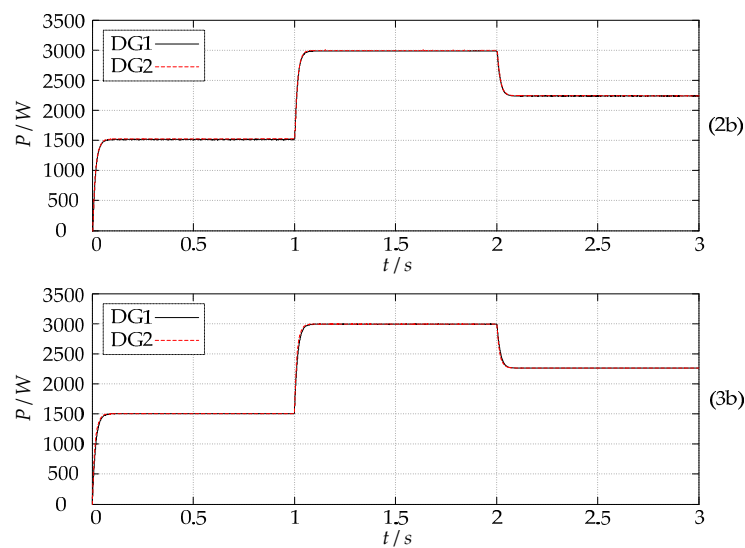


Figure 10. Simulation results of active power/DG voltage: method 1 (traditional method) using constant voltage amplitude reference; method 2 (proposed method) using CVAR; method 3 (proposed method) using improved active droop coefficient. (1a) DG voltage in method 1; (2a) DG voltage in method 2; (3a) DG voltage in method 3; (1b) DG active power output in method 1; (2b) DG active power output in method 2; (3b) DG active power output in method 3.

7. Conclusions

An improved P/U droop control strategy based on changeable reference is proposed for restoring frequency and improving active power sharing accuracy. In the case of load changes, DG running frequency can stabilize at the rated value (50 Hz) by changing frequency reference to compensate for frequency deviation while hardly influencing DG reactive power output. Thus, frequency restoration is realized by using CFR in the proposed method. Besides, to eliminate the influences of line inductance on active power sharing accuracy and power coupling, we use a virtual impedance method to design the inverter impedance as negative line inductance to neutralize line inductance. Then, we consider voltage drop in line impedance and give CVAR. Thus, actual droop lines corresponding to actual DG voltages can be obtained and will be used to control DGs so as to improve active power sharing accuracy. CVAR is further simplified as improving active droop coefficient. By using improved active droop coefficient to control DGs, active power sharing is still accurate and the performance of DG voltage stability will be better. Besides the control precision, the robust performance in the case of load changes or disturbances is also discussed. By proposing and using a robust control method based on the Lyapunov function in the inter-loop controller, robustness problems of frequency/voltage/powers are minimized. The simulation results coincide with the above theoretical results (i.e., the proposed method really contributes to frequency restoration and power accuracy improvement, with good robustness).

Acknowledgments: This work is supported by the National Natural Science Foundation of China under Grants 61573300 and 61533010, and Hebei Provincial Natural Science Foundation of China under Grant E2016203374.

Author Contributions: This paper was a collaborative effort among all authors. All authors conceived the methodology, conducted the experiments and wrote the paper.

Conflicts of Interest: The authors declare no conflict of interest.

Nomenclature

DGs	Distributed generation devices
CFR	Changeable frequency reference
LMI	Linear matrix inequality
P/U	DG active power output/DG voltage
CVAR	Changeable voltage amplitude reference
COT	Convex optimization techniques
PWM	Pulse width modulation

References

1. Liu, Z.; Su, C.; Hoidalén, H.; Chen, Z. A multi-agent system based protection and control scheme for distribution system with distributed generation integration. *IEEE Trans. Power Deliv.* **2017**, *32*, 536–545. [[CrossRef](#)]
2. Chang, C.C.; Gorinevsky, D.; Lall, S. Stability analysis of distributed power generation with droop inverters. *IEEE Trans. Power Syst.* **2015**, *30*, 3295–3303. [[CrossRef](#)]
3. Pathak, G.; Singh, B.; Panigrahi, B.K. Back-propagation algorithm-based controller for autonomous wind-DG microgrid. *IEEE Trans. Ind. Appl.* **2016**, *52*, 4408–4415. [[CrossRef](#)]
4. Che, L.; Zhang, X.; Shahidehpour, M.; Alabdulwahab, A.; Al-Turki, Y. Optimal planning loop-based microgrid topology. *IEEE Trans. Smart Grid* **2017**, *8*, 1771–1781. [[CrossRef](#)]
5. Wang, H.; Huang, J. Joint investment and operation of microgrid. *IEEE Trans. Smart Grid* **2017**, *8*, 833–845. [[CrossRef](#)]
6. Guo, W.; Mu, L.; Zhang, X. Fault models of inverter-interfaced distributed generators within a low-voltage microgrid. *IEEE Trans. Power Deliv.* **2017**, *32*, 453–461. [[CrossRef](#)]
7. Cingoz, F.; Elrayyah, A.; Sozer, Y. Plug-and-play nonlinear droop construction scheme to optimize islanded microgrid operations. *IEEE Trans. Power Electron.* **2017**, *32*, 2743–2756. [[CrossRef](#)]
8. Karavas, C.S.; Kyriakarakos, G.; Arvanitis, K.G.; Papadakis, G. A multi-agent decentralized energy management system based on distributed intelligence for the design and control of autonomous polygeneration microgrids. *Energy Convers. Manag.* **2015**, *103*, 166–179. [[CrossRef](#)]
9. Hatziargyriou, N.; Asano, H.; Iravani, R.; Marnay, C. Microgrids. *IEEE Power Energy Mag.* **2007**, *5*, 78–94. [[CrossRef](#)]
10. Kyriakarakos, G.; Dounis, A.I.; Rozakis, S.; Arvanities, K.G.; Papadakis, G. Polygeneration microgrids: A viable solution in remote areas for supplying power, potable water and hydrogen as transportation fuel. *Appl. Energy* **2011**, *88*, 4517–4526. [[CrossRef](#)]
11. Han, H.; Hou, X.; Yang, J.; Wu, J. Review of power sharing control strategies for islanding operation of ac microgrids. *IEEE Trans. Smart Grid* **2016**, *7*, 200–215. [[CrossRef](#)]
12. Wang, X.; Blaabjerg, F.; Chen, Z. Autonomous control of inverter-interfaced distributed generation units for harmonic filtering and resonance damping in an islanded microgrid. *IEEE Trans. Ind. Appl.* **2014**, *50*, 452–461. [[CrossRef](#)]
13. Dou, C.; Zhang, Z.; Yue, D.; Song, M. Improved droop control based on virtual impedance and virtual power source in low-voltage microgrid. *IET Gener. Transm. Distrib.* **2017**, *11*, 1046–1054. [[CrossRef](#)]
14. Sun, X.; Hao, Y.; Wu, Q.; Guo, X. A multifunctional and wireless droop control for distributed energy storage units in islanded AC microgrid applications. *IEEE Trans. Power Electron.* **2016**, *32*, 736–751. [[CrossRef](#)]
15. Yu, K.; Ai, Q.; Wang, S.; Ni, J. Analysis and optimization of droop controller for microgrid system based on small-signal dynamic model. *IEEE Trans. Smart Grid* **2016**, *7*, 695–705. [[CrossRef](#)]
16. Marinovici, L.D.; Lian, J.; Kalsi, K.; Du, P. Distributed hierarchical control architecture for transient dynamics improvement in power systems. *IEEE Trans. Power Syst.* **2013**, *28*, 3065–3074. [[CrossRef](#)]
17. Li, Y.W.; Kao, C.N. An accurate power control strategy for power-electronics-interfaced distributed generation units operating in a low-voltage multibus microgrid. *IEEE Trans. Power Electron.* **2009**, *24*, 2977–2988.
18. Mahmood, H.; Michaelson, D.; Jiang, J. Accurate reactive power sharing in an islanded microgrid using adaptive virtual impedances. *IEEE Trans. Power Electron.* **2015**, *30*, 1605–1617. [[CrossRef](#)]

19. Han, Y.; Shen, P.; Zhao, X.; Guerrero, J.M. An enhanced power sharing scheme for voltage unbalance and harmonics compensation in an islanded microgrid. *IEEE Trans. Energy Convers.* **2016**, *31*, 1037–1050. [[CrossRef](#)]
20. Guo, F.; Wen, C.; Mao, J.; Song, Y.D. Distributed secondary voltage and frequency restoration control of droop-controlled inverter-based microgrids. *IEEE Trans. Ind. Electron.* **2015**, *62*, 4355–4364. [[CrossRef](#)]
21. Zuo, S.; Davoudi, A.; Song, Y.; Lewis, F.L. Distributed finite-time voltage and frequency restoration in islanded ac microgrids. *IEEE Trans. Ind. Electron.* **2016**, *63*, 5988–5997. [[CrossRef](#)]
22. Kim, Y.S.; Kim, E.S.; Moon, S.I. Distributed generation control method for active power sharing and self-frequency recovery in an islanded microgrid. *IEEE Trans. Power Syst.* **2017**, *32*, 544–551. [[CrossRef](#)]
23. Vandoorn, T.L.; De Kooning, J.D.M.; Meersman, B.; Guerrero, J.M. Automatic power-sharing modification of P/V droop controllers in low-voltage resistive microgrids. *IEEE Trans. Power Deliv.* **2012**, *27*, 2318–2325. [[CrossRef](#)]
24. He, J.; Li, Y.W.; Guerrero, J.M.; Blaabjerg, F.; Vasquez, J.C. An islanding microgrid power sharing approach using enhanced virtual impedance control scheme. *IEEE Trans. Power Electron.* **2013**, *28*, 5272–5282. [[CrossRef](#)]
25. Zhu, Y.; Zhuo, F.; Wang, F.; Liu, B. A virtual impedance optimization for reactive power sharing in networked microgrid. *IEEE Trans. Power Electron.* **2016**, *31*, 2890–2904. [[CrossRef](#)]
26. He, J.; Li, Y.W. An enhanced microgrid load demand sharing strategy. *IEEE Trans. Power Electron.* **2012**, *27*, 3984–3995. [[CrossRef](#)]
27. Sao, C.K.; Lehn, P.W. Autonomous load sharing of voltage source converters. *IEEE Trans. Power Deliv.* **2005**, *20*, 1009–1016. [[CrossRef](#)]
28. Zhang, P.; Zhao, H.; Cai, H.; Shi, J. Power decoupling strategy based on ‘virtual negative resistor’ for inverters in low-voltage microgrids. *IET Power Electron.* **2016**, *9*, 1037–1044. [[CrossRef](#)]
29. Li, B.; Zhou, L.; Yu, X.; Zheng, C.; Liu, J. Improved power decoupling control strategy based on virtual synchronous generator. *IET Power Electron.* **2017**, *10*, 462–470. [[CrossRef](#)]
30. Wu, X.; Shen, C.; Iravani, R. Feasible range and optimal value of the virtual impedance for droop-based control of microgrids. *IEEE Trans. Smart Grid* **2017**, *8*, 1242–1251. [[CrossRef](#)]
31. Han, Y.; Shen, P.; Zhao, X.; Guerrero, J.M. Control strategies for islanded microgrid using enhanced hierarchical control structure with multiple current-loop damping schemes. *IEEE Trans. Smart Grid* **2017**, *8*, 1139–1153. [[CrossRef](#)]



© 2017 by the authors. Licensee MDPI, Basel, Switzerland. This article is an open access article distributed under the terms and conditions of the Creative Commons Attribution (CC BY) license (<http://creativecommons.org/licenses/by/4.0/>).